UNITED STATES DEPARTMENT OF THE INTERIOR

GEOLOGICAL SURVEY

A MAGNETOTELLURIC STUDY OF THE STILLWATER-SODA LAKES, NEVADA GEOTHERMAL AREA

By

W. D. Stanley, R. R. Wahl, J. G. Rosenbaum

Open-File Report 76-80
1976

This report is preliminary
and has not been edited
or reviewed for conformity
to Geological Survey standards.

A MAGNETOTELLURIC STUDY OF THE STILLWATER-SODA LAKES, NEVADA GEOTHERMAL AREA

By W. D. Stanley, R. R. Wahl, J. G. Rosenbaum

INTRODUCTION

The Stillwater-Soda Lakes K.G.R.A. (Known Geothermal Resource area) is located in the Carson Desert of west central Nevada, near the town of Fallon (figure 1). Two thermal areas have been mapped by shallow drilling. Near the farming community of Stillwater, an area of about 70 km^2 has been mapped with groundwater hotter than 20^o C and as hot as 80^o C or slightly hotter in the center of the anomaly (Olmstead, et. al., 1975). The MT method was selected as a tool to study the geothermal area, both to define the extent of the mapped thermal anomalies and to determine the broader nature of the thermal regime and possibly the source of the anomalous heat flow.

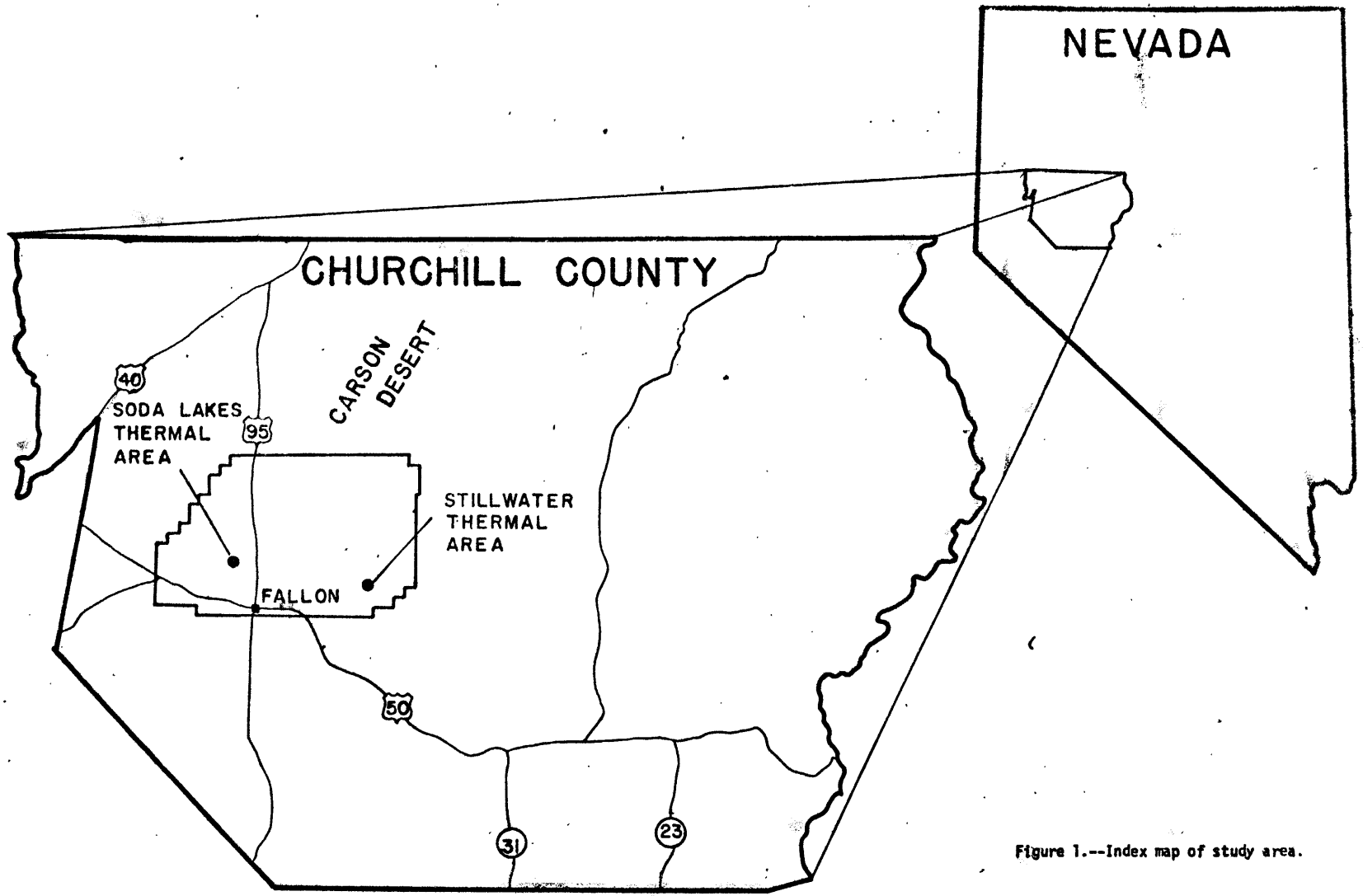

Figure 1.--Index map of study area.

Magnetotelluric Measurements

MT soundings were made at twenty-five sites on four profiles in the study area. Mu-metal cored induction coils were used to measure the orthogonal magnetic field components H_x, H_y, and H_z. Potential dipoles of 100 m length with cadmium chloride porous pots as electrodes were used to measure the orthogonal electric fields E_x and E_y. Data were recorded on 1/2" tape with 12 bit digitization under minicomputer control; recordings were made over up to 4 bands from 0.002 to 256 Hz. For ten of the stations (2-1 through 2-10) the lowest frequency band with corner frequencies at 0.002 and 0.05 Hz (Band 2) was included with the three higher frequency bands shown in Table 1, (Bands 3-6) but for the remaining 15 stations (1-1 through 1-15) this band was not included.

TABLE 1

BAND	CORNER FREQ.	NO OF RUNS	SAMPLE RATE	RUN LENGTH
B6	10 - 256 Hz	4	1024/sec	4 sec
B5	1 - 25 Hz	4	128/sec	32 sec
B4	0.1 - 5 Hz	2	32/sec	128 sec
B3	0.01 - 0.5 Hz	2	2/sec	34 min, 8 sec
B2	0.002 - 0.125 Hz	1	0.5/sec	2 Hrs, 16 min, 32 sec
B1	0.002 - 0.025 Hz	Not used	-----	-----

Each run shown in table 1 consisted of 4096 samples to give the run times indicated.

DATA PROCESSING

Five channel data for the three magnetic and two electric fields measured were processed as outlined in the flow chart of figure 2. The five channels of magnetotelluric data, h_x, h_y, h_z, e_x, e_y (small letters denote times series) were recorded as digital time series using three induction coils for the magnetic fields and potential dipoles for the electric fields. Processing of the time series to obtain tensor resistivities has been described in detail (Sims, et. al., 1971 ; Word, et. al., 1969) elsewhere and we present only the pertinent sequence of steps required in the processing.

The first step in processing is to obtain the five time series by demultiplexing the channel data and header information on the field tape. The various runs are then selectively edited (see Table 1). As many good run files are selected as is possible for spectral averaging. Next the discrete Fourier transforms for the five channels are obtained through use of the FFT (Fast Fourier Transform) algorithm. We denote the Fourier coefficients of the data channels by capitol letters, thus the transform pairs are:

$$H_x \overleftrightarrow{\to} h_x$$

$$H_y \overleftrightarrow{\to} h_y$$

$$H_z \overleftrightarrow{\to} h_z$$

$$E_x \overleftrightarrow{\to} e_x$$

$$E_y \overleftrightarrow{\to} e_y$$

The earth can be considered a linear system where the frequency domain coefficients of the horizontal electric and magnetic fields are related

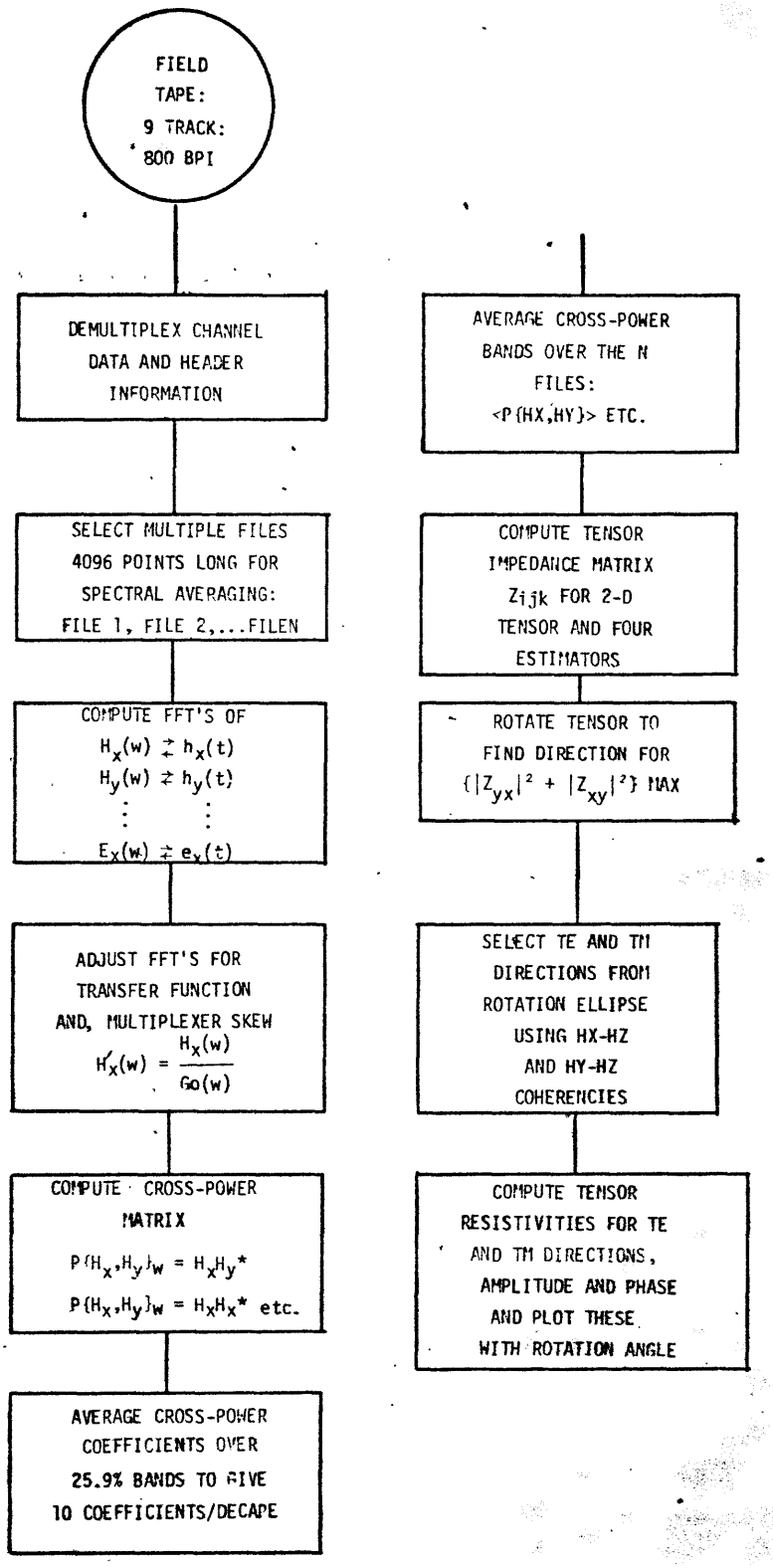

Figure 2.--Flow chart for magnetotelluric data processing.

by a tensor of rank two for a two-dimensional earth.

(1) $E_x = H_x Z_{xx} + H_y Z_{xy}$

(2) $E_y = H_x Z_{xy} + H_y Z_{xx}$

If we compute the cross power spectra of (1) with all possible horizontal components we obtain:

(3) $E_x E_x^* = H_x E_x^* Z_{xx} + H_y E_x^* Z_{xy}$

(4) $E_x E_y^* = H_x E_y^* Z_{xx} + H_y E_y^* Z_{xy}$

(5) $E_x H_x^* = H_x H_x^* Z_{xx} + H_y H_x^* Z_{xy}$

(6) $E_x H_y^* = H_x H_y^* Z_{xx} + H_y H_y^* Z_{xy}$

Equations (3) through (6) can be grouped into six pairs of equation to solve for Z_{xx} and Z_{xy}. Two of the pairs are unstable for a horizontal earth since their determinants are:

$$(H_x E_x^*)(H_y H_y^*) - (H_x H_y^*)(H_y E_x^*)$$

and $$(H_x E_y^*)(H_y H_x^*) - (H_x H_x^*)(H_y E_y^*)$$

Similarly we can take cross-powers of (2) to arrive at six pairs of equations to solve for Z_{yy} and Z_{xy} two of which are indeterminate for a 1-D earth. The remaining pairs lead to four different estimators for Z_{ij}. It can be shown (Sims, et. al., 1971) that averaging the cross-powers, $E_x E_y^*$, etc., over more than one data set leads to least square minimum error solution for Z_{ij}. In addition the Z_{ij} are considered to be slowly varying with frequency and can be computed for logarithmically spaced frequencies, thus the cross spectra are computed over these frequency bands by summing incremental components before the linear equations are solved. For this survey the frequency bands were 25.9 percent bands, giving 10 points per log cycle.

The tensor elements are then rotated to find the principal impedance axes, which will exist in the data over some frequency ranges if the earth approximates two-dimensionality at those frequencies. The principal directions are found by computing the angle which maximizes $(|Z_{xy}|^2 + |Z_{yx}|^2)$, or alternately, minimizes $(|Z_{xx}|^2 + |Z_{yy}|^2)$. The distinction of the principal directions into TE and TM modes is done by calculating the directions for maximum coherency of H_z with H_x and H_y. For a two dimensional earth one of the principal directions obtained by Z_{ij} rotation should align with the TE direction, which is the direction for maximum H_x-H_z coherency. The departure from the angle computed by the two different rotations is a measure of three-dimensionality.

Tensor resistivities are computed from the surface impedance relationship:

$$\rho_{ij} = 0.2T|Z_{ij}|^2$$

where T is the period in seconds for the given frequency band.

The tensor resistivity amplitude and phase are plotted if the phasor coherency for a particular frequency band is high enough. Phasor coherency is a parameter defined as:

$$\text{Phasor Coherency} = C_\eta = 1 - \frac{Z_\eta}{\sum Z_i} \qquad i=1,N$$

where Z_η is one of the N possible estimates and C_η is the coherency for that estimate. The range of C_η is: $-\infty<C_\eta<1$. If all the estimates are identical, then the phasor coherency will be unity. In general, nonunity coherency is due to measurement system noise, ambient noise, etc. In fact, two of the estimates are biased down by random noise on H and are not biased by random noise on E, whereas the other two are biased up by random noise on E and are not biased by random noise on H. Thus, for about equal random or incoherent noise on E and H, an average of the four estimates should prove to be best estimate. However, if the noise can be identified as mostly on E or mostly on H, the appropriate estimates may be used.

In this survey, points were plotted if the phasor coherency was greater than 0.8, with some points used in the range 0.5-0.8 on extremely bad sets of data such as a few of the "high frequency" soundings.

Plots of amplitude and phase of the tensor resistivities are shown in figures 3a to 3j for stations 2-1 through 2-10. In most instances the resistivity curves are reasonably well defined by the multiplicity of points from the various overlapping bands. The figures show TM (transverse magnetic) curves which we have hand smoothed through the data as dashed lines, whereas the solid curves are the computer generated curves for one-dimensional models obtained using a generalized inversion program (B. Smith, U.S.G.S., written comm) to fit the amplitude curves. We modeled the TE curves because the TE values are less distorted than the TM by two-dimensional features. For three-dimensionalities, this is not true, of course, but one-dimensional inversion yields a readily obtainable first approximation to the geological structures. In most cases the expense and time required for extensive two-dimensional modeling is not justified. Sketching of the TM and TE resistivity curves was aided by alphanumeric plotting symbols, with different symbols being used for each band and principal direction. These symbols are not distinguishable in the reduced versions of the computer plots of figure 3.

Several of the data sets show a large split between the TE and TM directions, particularly 2-1, 2-7,2-8, and 2-10. This apparent two-dimensionality (and to some degree, three-dimensionality) agrees with known geology and with our gross one-dimensional inversions to be discussed below.

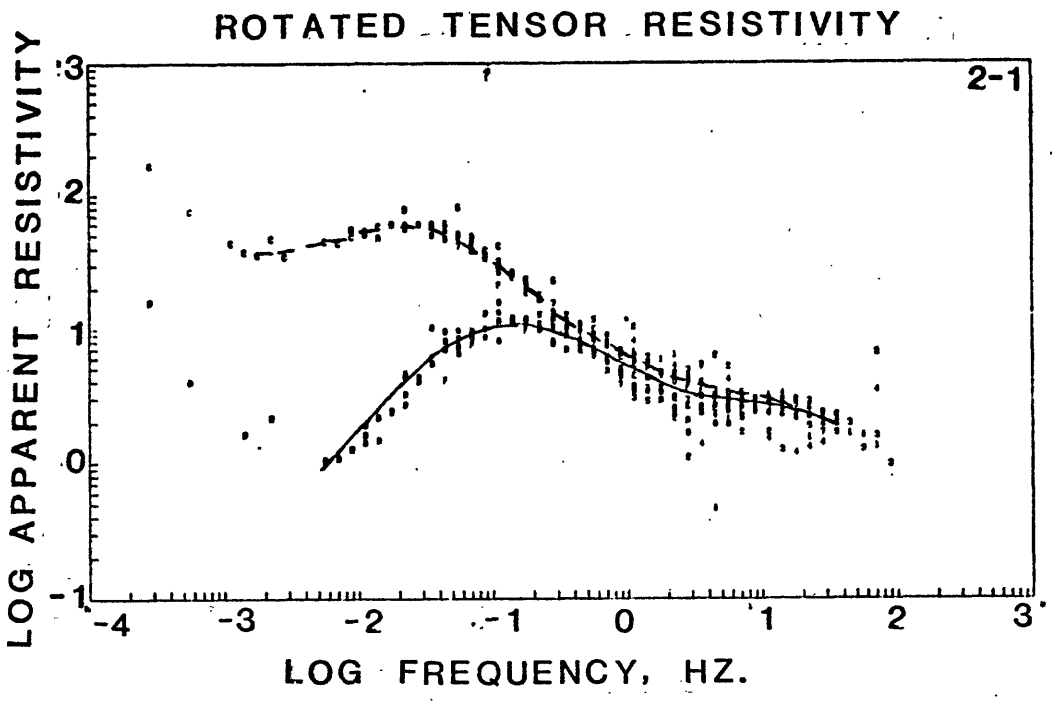

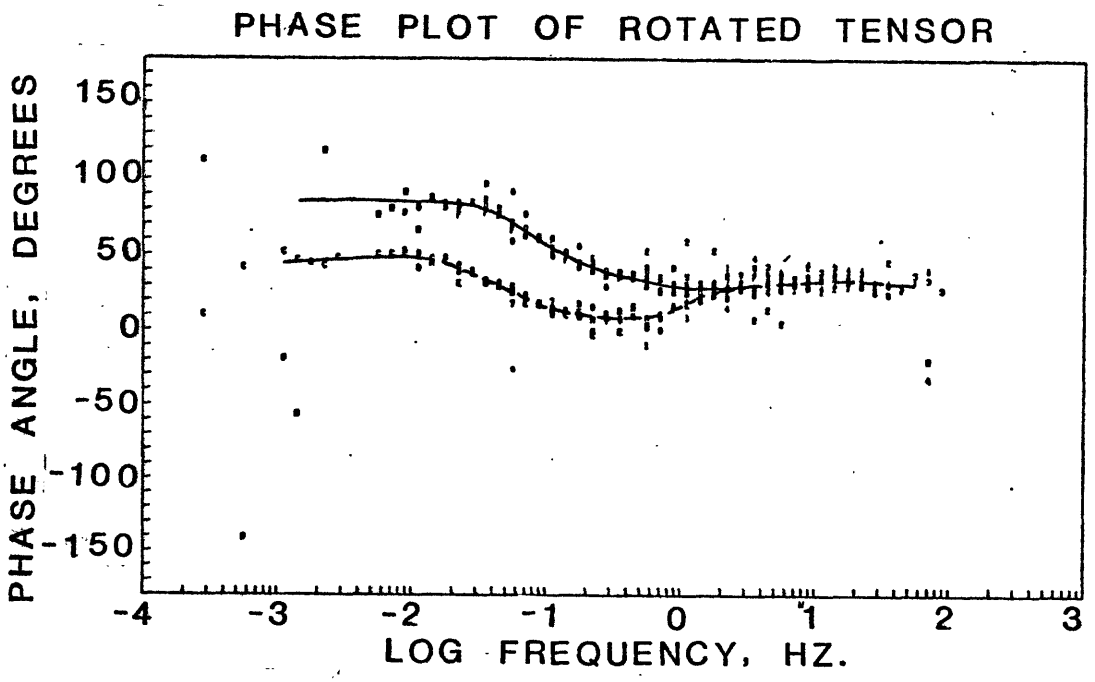

Figure 3.--Tensor resistivity amplitude and phase data for MT sites 2-1 to 2-10. Solid curves on amplitude are computer generated curves for TE models. Dashed lines are hand smoothed fits to TM data. Horizontal axes are log frequency, vertical axes are tensor apparent resistivity amplitude and phase.

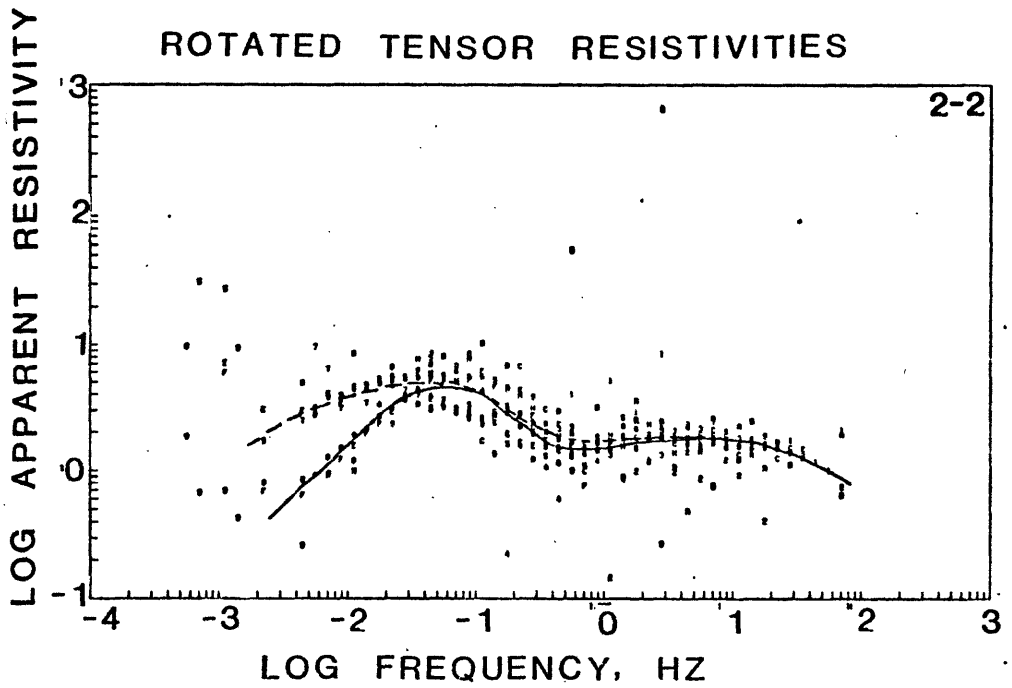
ROTATED TENSOR RESISTIVITIES
2-2
LOG APPARENT RESISTIVITY
3
2
1
0
-1
-4
-3
-2
-1
0
1
2
3
LOG FREQUENCY, HZ

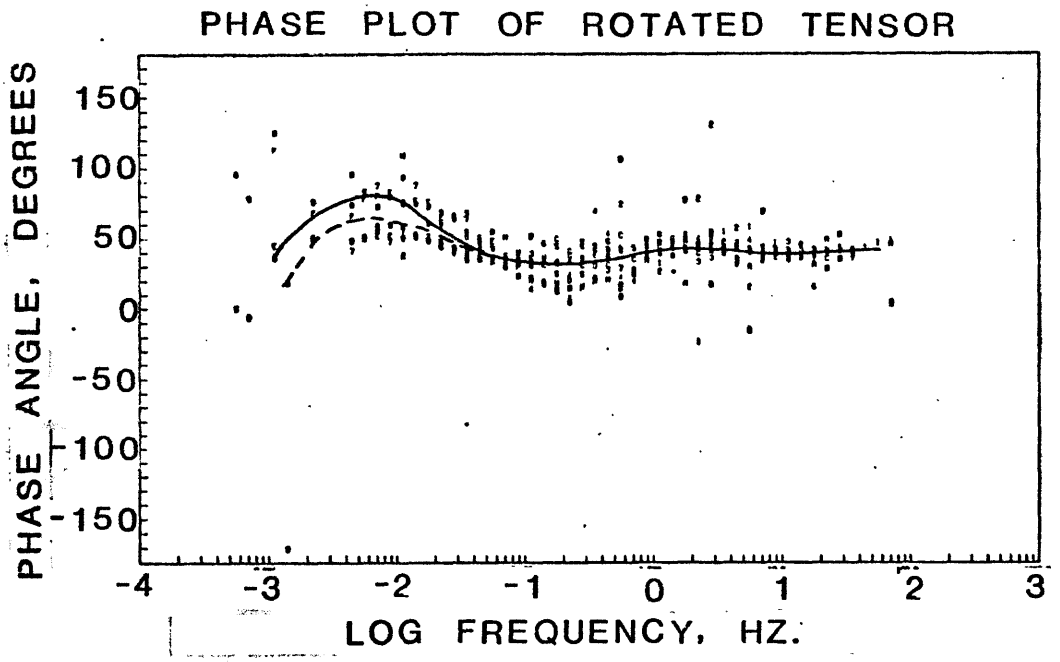
PHASE PLOT OF ROTATED TENSOR
PHASE ANGLE, DEGREES
150
100
50
0
-50
-100
-150
-4
-3
-2
-1
0
1
2
3
LOG FREQUENCY, HZ.

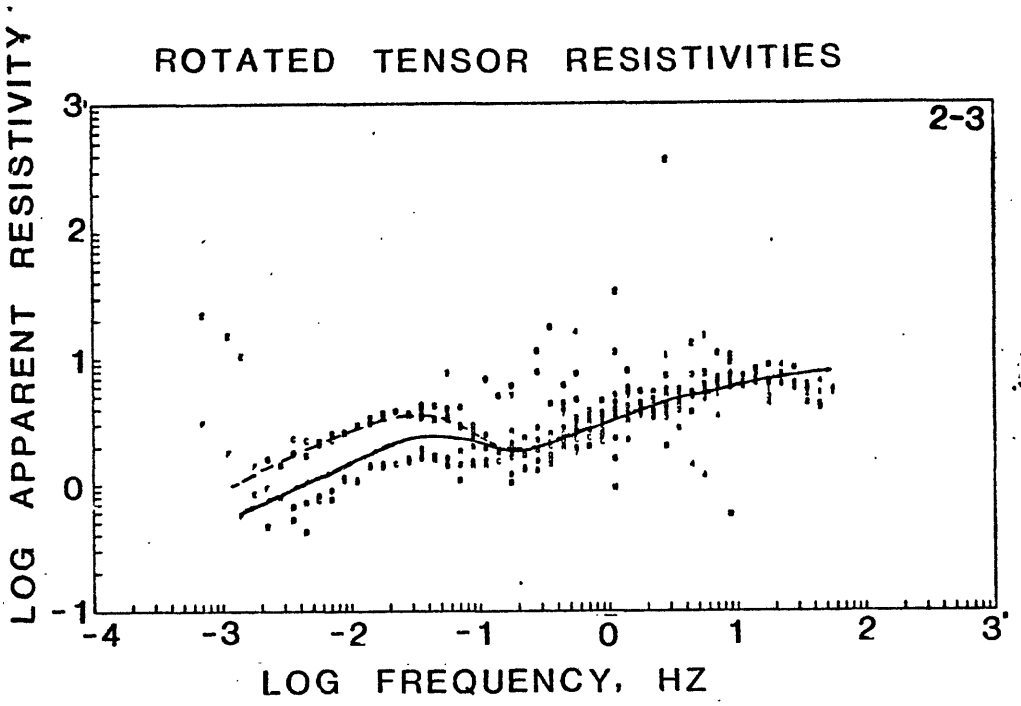
ROTATED TENSOR RESISTIVITIES
2-3
LOG APPARENT RESISTIVITY
3
2
1
0
-1
-4
-3
-2
-1
0
1
2
3
LOG FREQUENCY, HZ

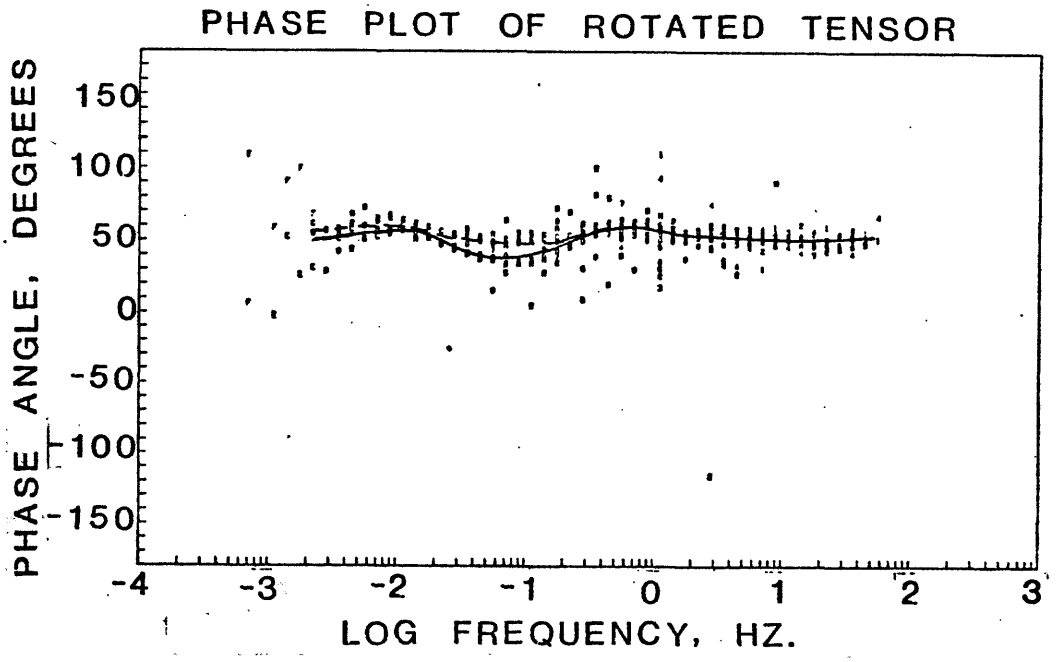
PHASE PLOT OF ROTATED TENSOR
PHASE ANGLE, DEGREES
150
100
50
0
-50
-100
-150
-4
-3
-2
-1
0
1
2
3
LOG FREQUENCY, HZ.

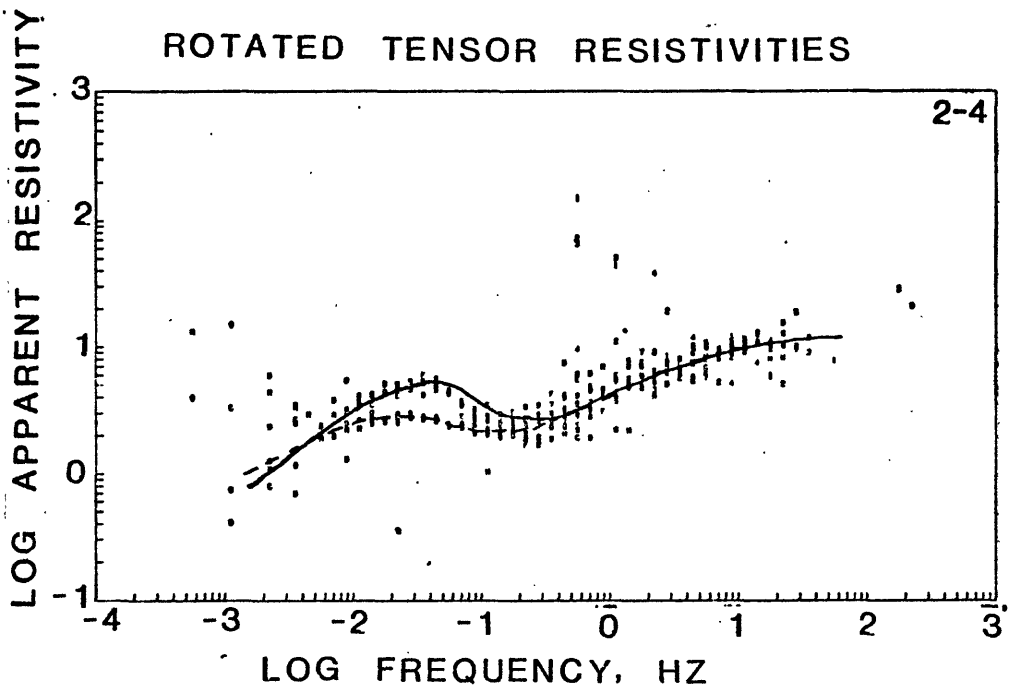
ROTATED TENSOR RESISTIVITIES
2-4
LOG APPARENT RESISTIVITY
3
2
1
0
-1
-4
-3
-2
-1
0
1
2
3
LOG FREQUENCY, HZ

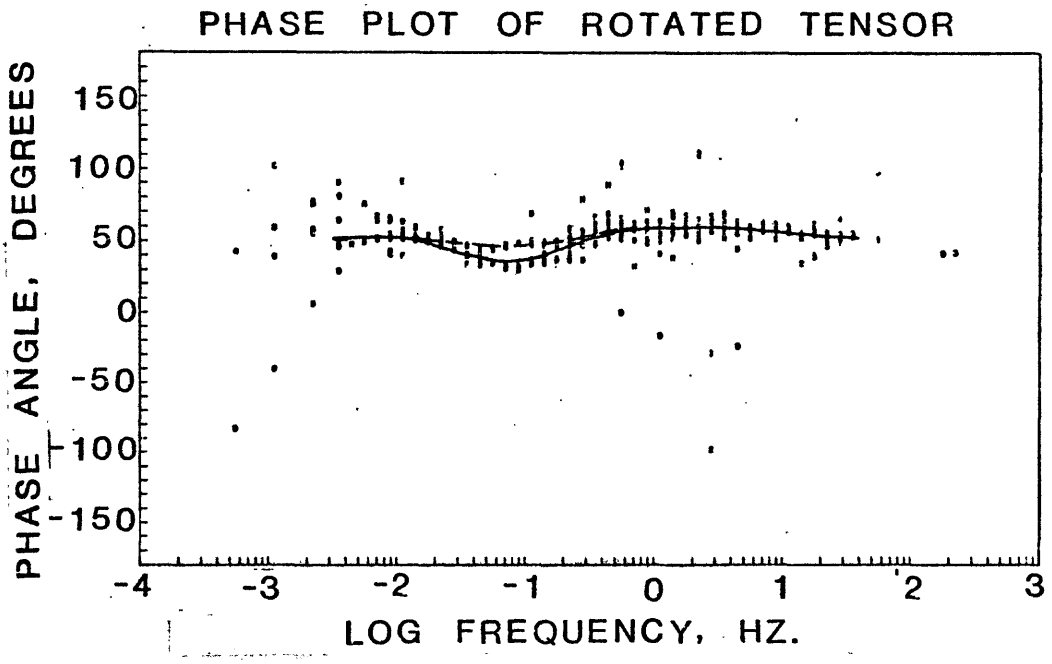
PHASE PLOT OF ROTATED TENSOR
PHASE ANGLE, DEGREES
150
100
50
0
-50
-100
-150
-4
-3
-2
-1
0
1
2
3
LOG FREQUENCY, HZ.

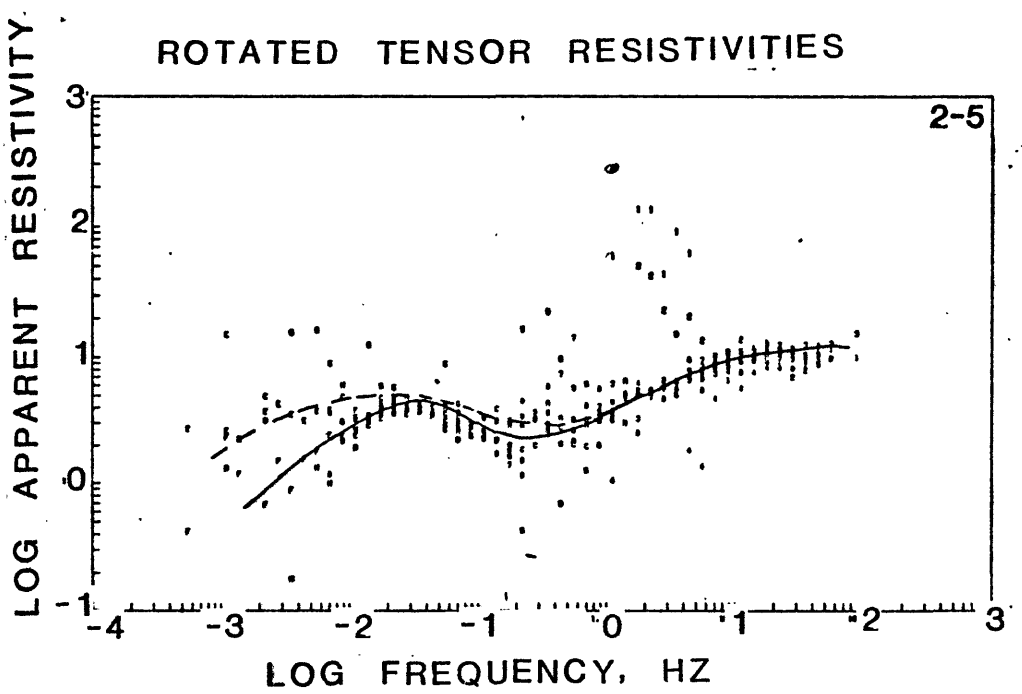
ROTATED TENSOR RESISTIVITIES
2-5
LOG APPARENT RESISTIVITY
3
2
1
0
-1
-4
-3
-2
-1
0
1
2
3
LOG FREQUENCY, HZ

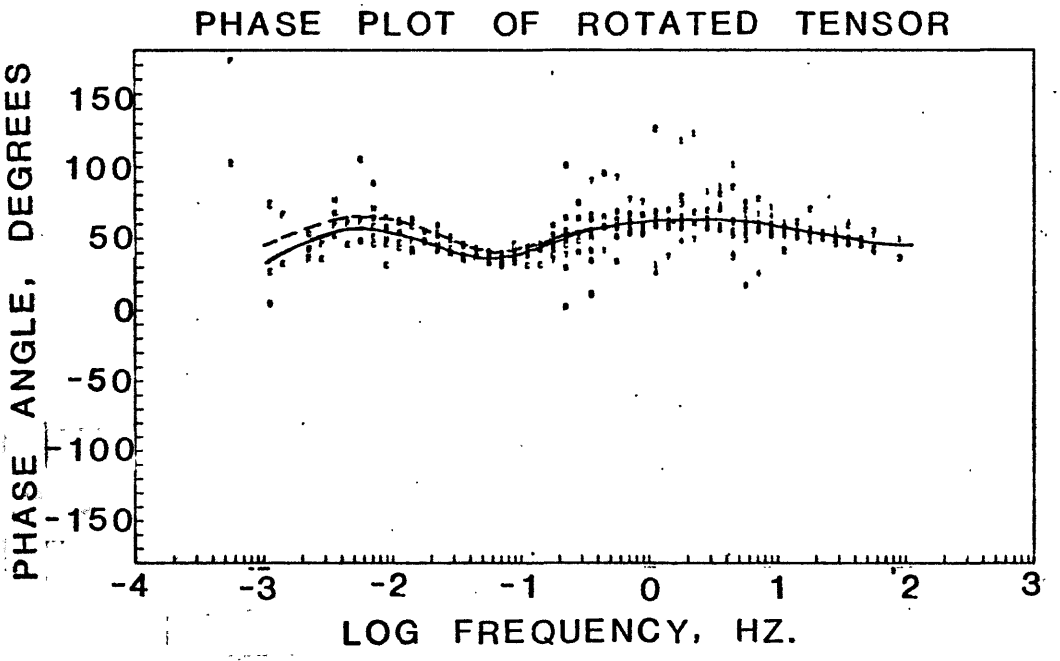
PHASE PLOT OF ROTATED TENSOR
PHASE ANGLE, DEGREES
150
100
50
0
-50
-100
-150
-4
-3
-2
-1
0
1
2
3
LOG FREQUENCY, HZ.

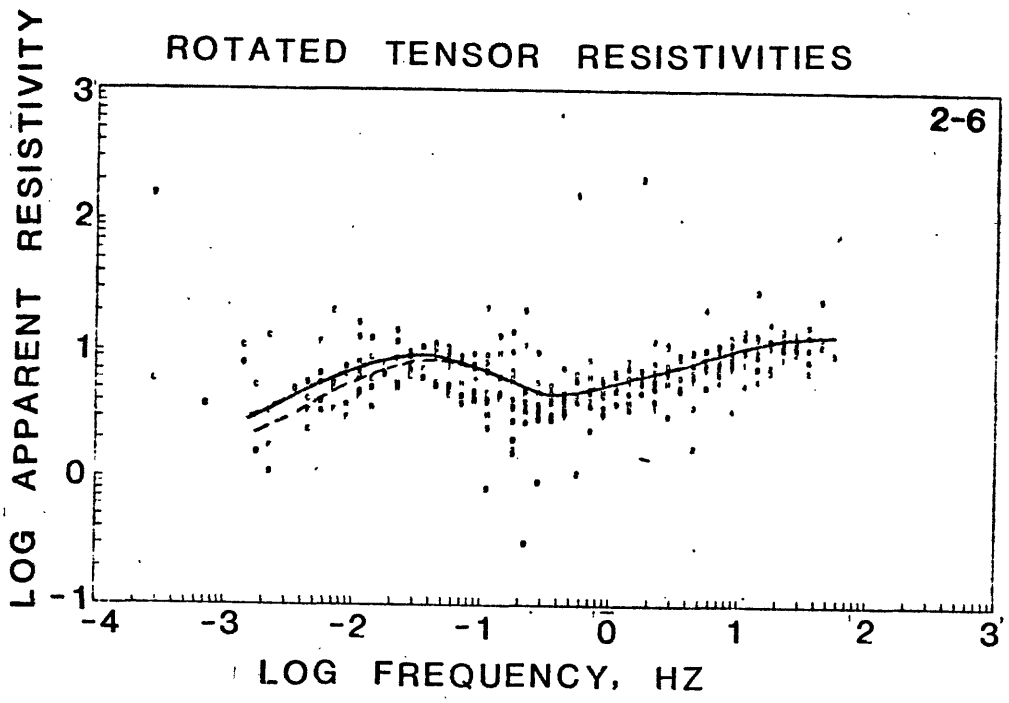
ROTATED TENSOR RESISTIVITIES
2-6
LOG APPARENT RESISTIVITY
3
2
1
0
-1
-4
-3
-2
-1
0
1
2
3
LOG FREQUENCY, HZ

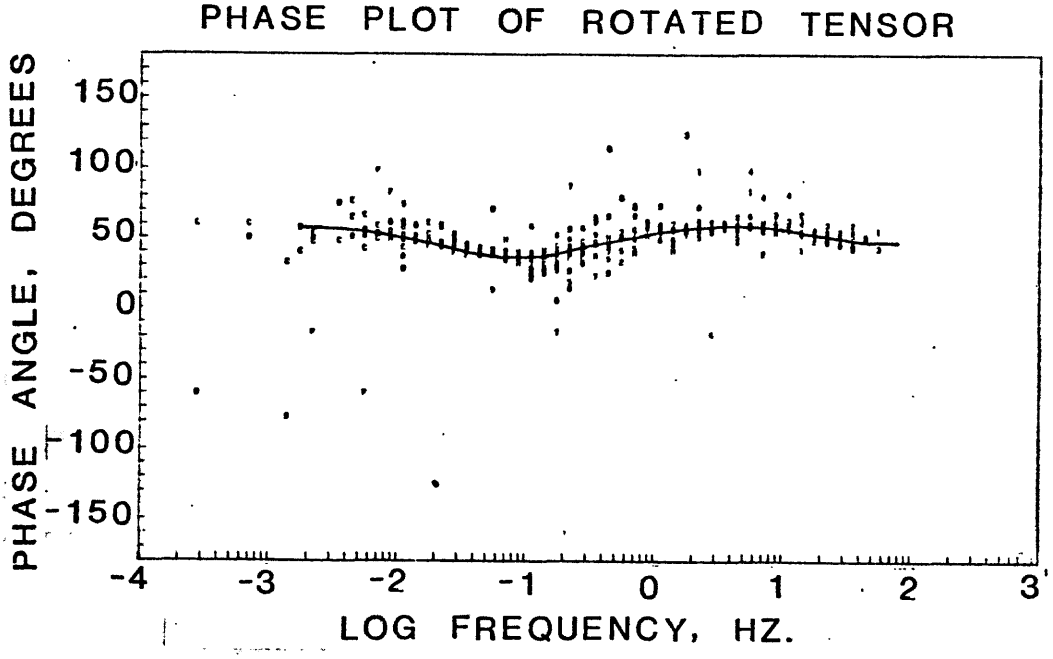
PHASE PLOT OF ROTATED TENSOR
PHASE ANGLE, DEGREES
150
100
50
0
-50
-100
-150
-4
-3
-2
-1
0
1
2
3
LOG FREQUENCY, HZ.

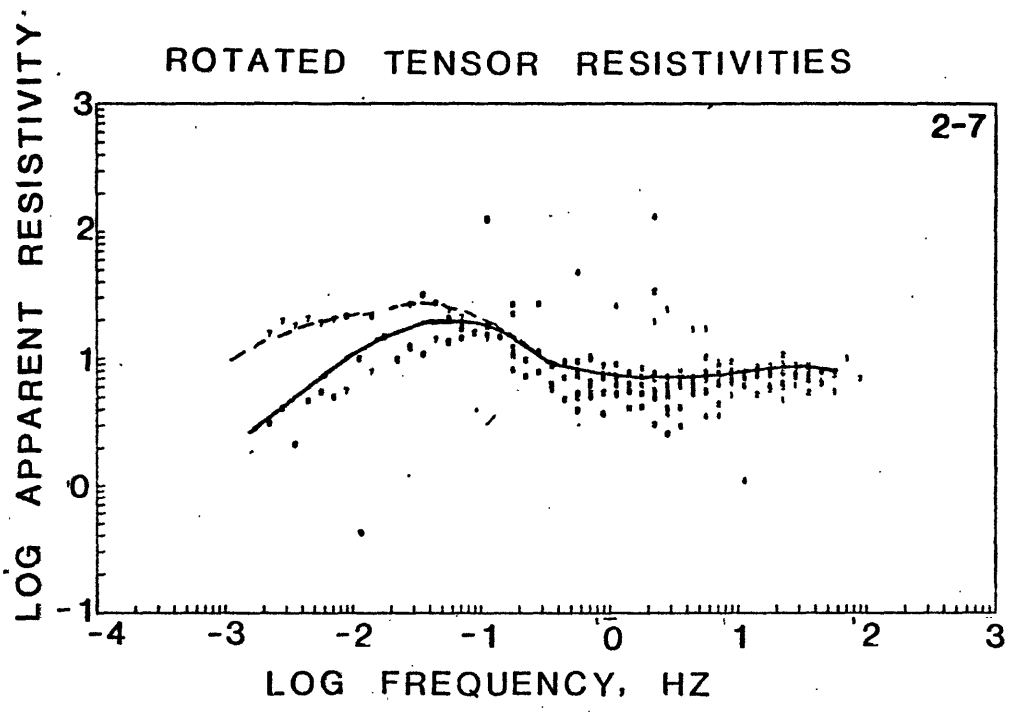
ROTATED TENSOR RESISTIVITIES
2-7
LOG APPARENT RESISTIVITY
3
2
1
0
-1
-4
-3
-2
-1
0
1
2
3
LOG FREQUENCY, HZ

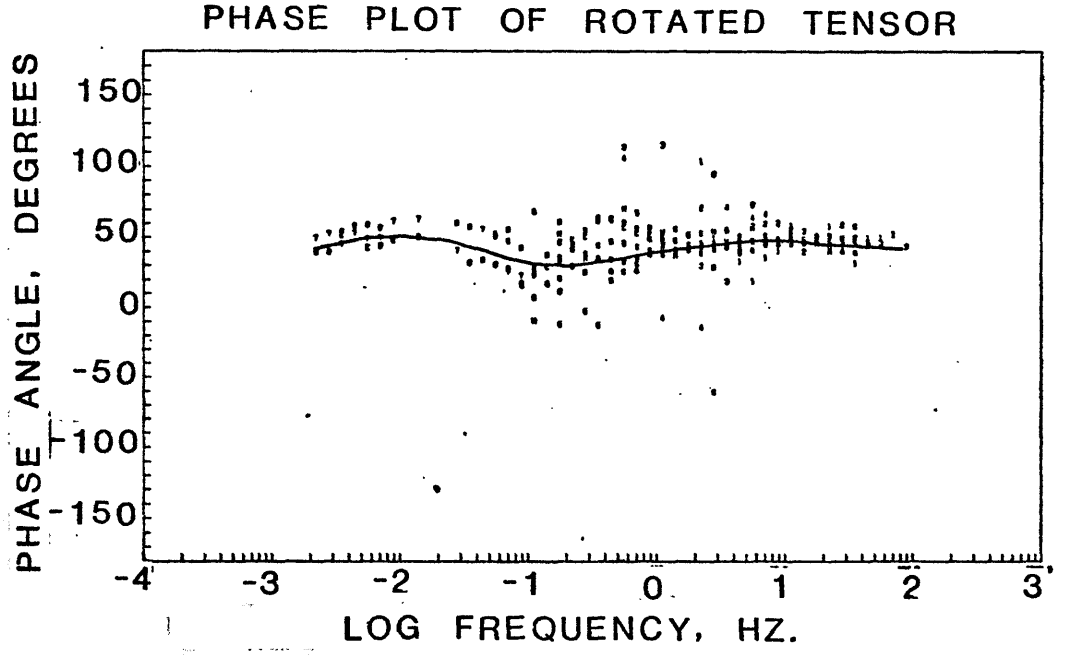
PHASE PLOT OF ROTATED TENSOR
PHASE ANGLE, DEGREES
150
100
50
0
-50
-100
-150
-4
-3
-2
-1
0
1
2
3
LOG FREQUENCY, HZ.

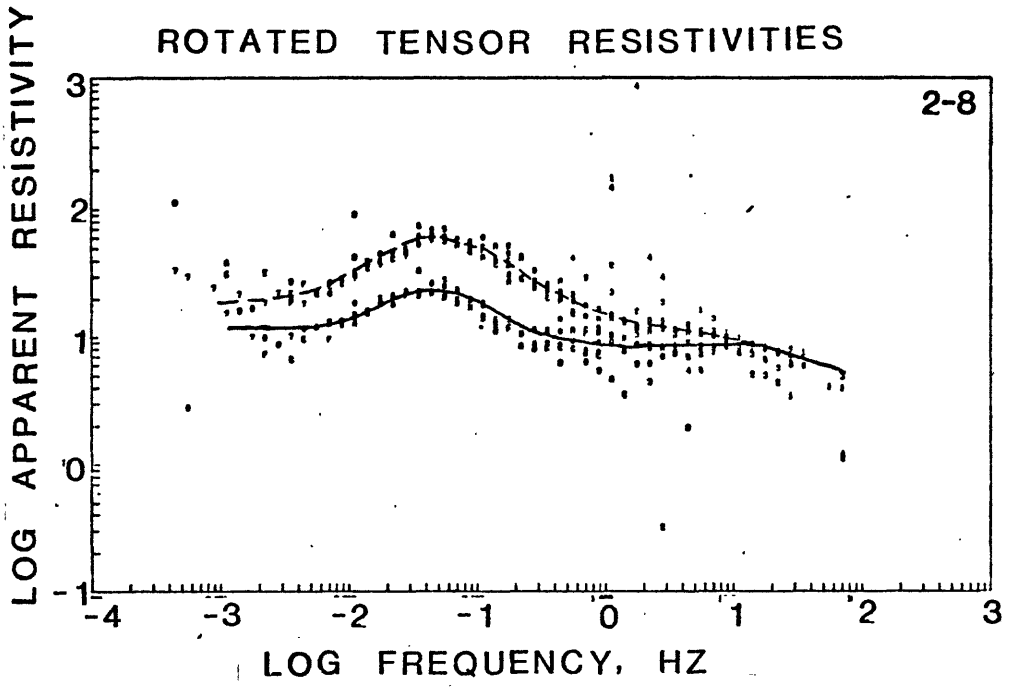
ROTATED TENSOR RESISTIVITIES
2-8
LOG APPARENT RESISTIVITY
3
2
1
0
-1
-4
-3
-2
-1
0
1
2
3
LOG FREQUENCY, HZ

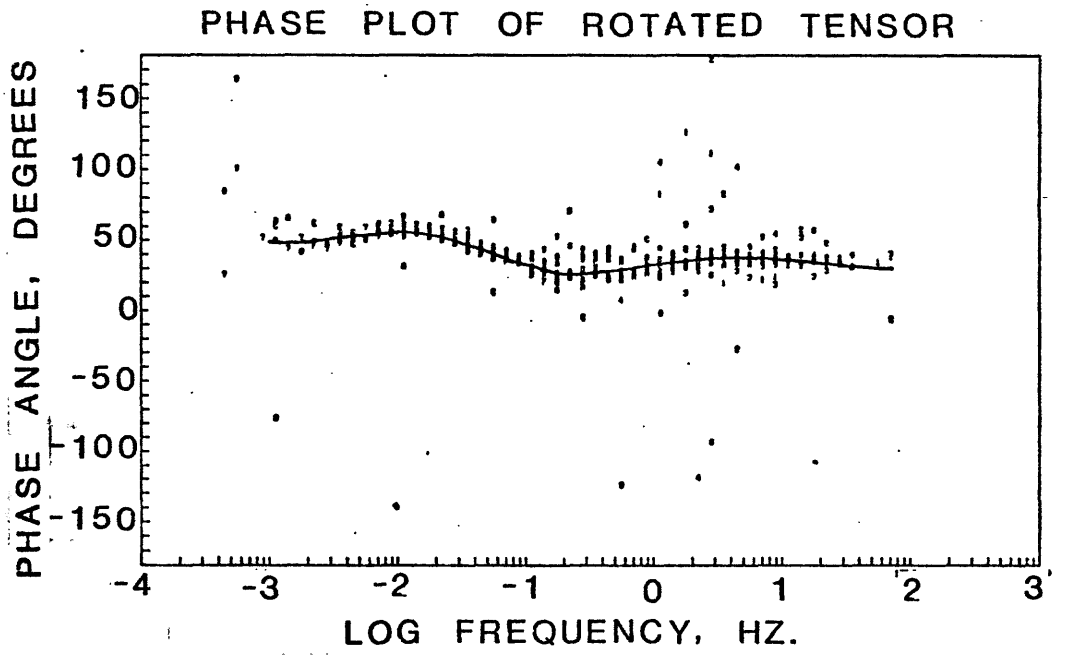
PHASE PLOT OF ROTATED TENSOR
PHASE ANGLE, DEGREES
150
100
50
0
-50
-100
-150
-4
-3
-2
-1
0
1
2
3
LOG FREQUENCY, HZ.

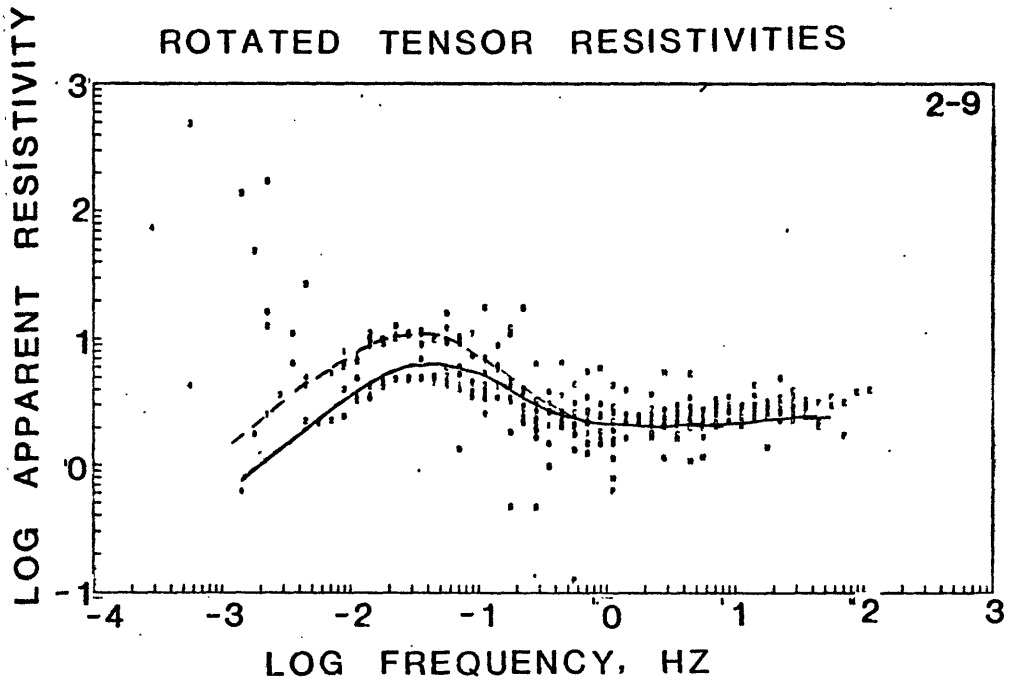
ROTATED TENSOR RESISTIVITIES
2-9
LOG APPARENT RESISTIVITY
3
2
1
0
-1
-4
-3
-2
-1
0
1
2
3
LOG FREQUENCY, HZ

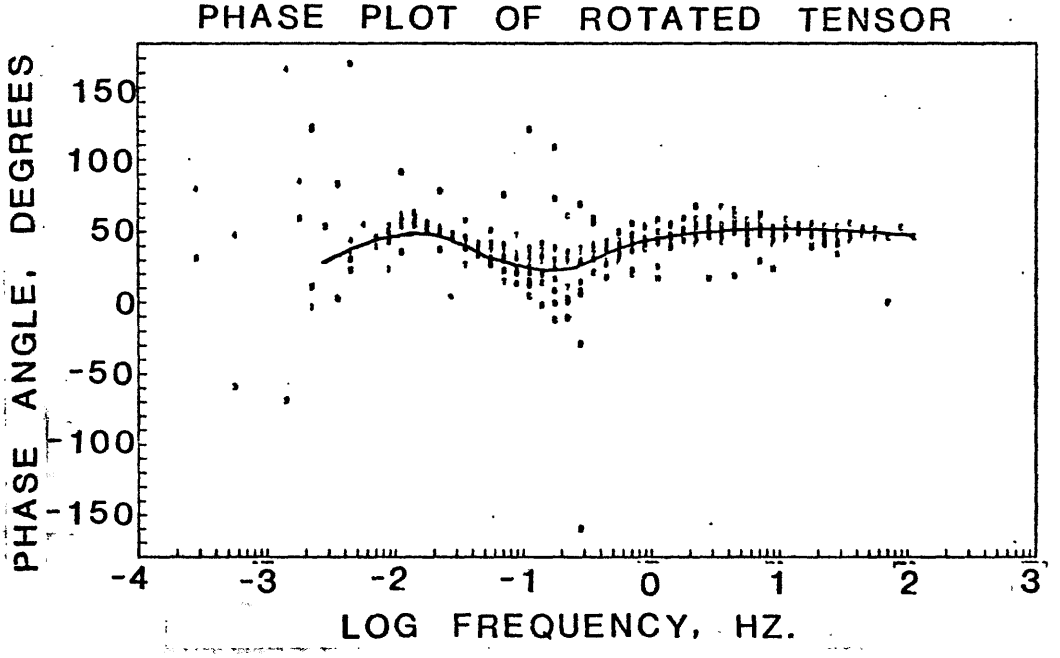
PHASE PLOT OF ROTATED TENSOR
PHASE ANGLE, DEGREES
150
100
50
0
-50
-100
-150
-4
-3
-2
-1
0
1
2
3
LOG FREQUENCY, HZ.

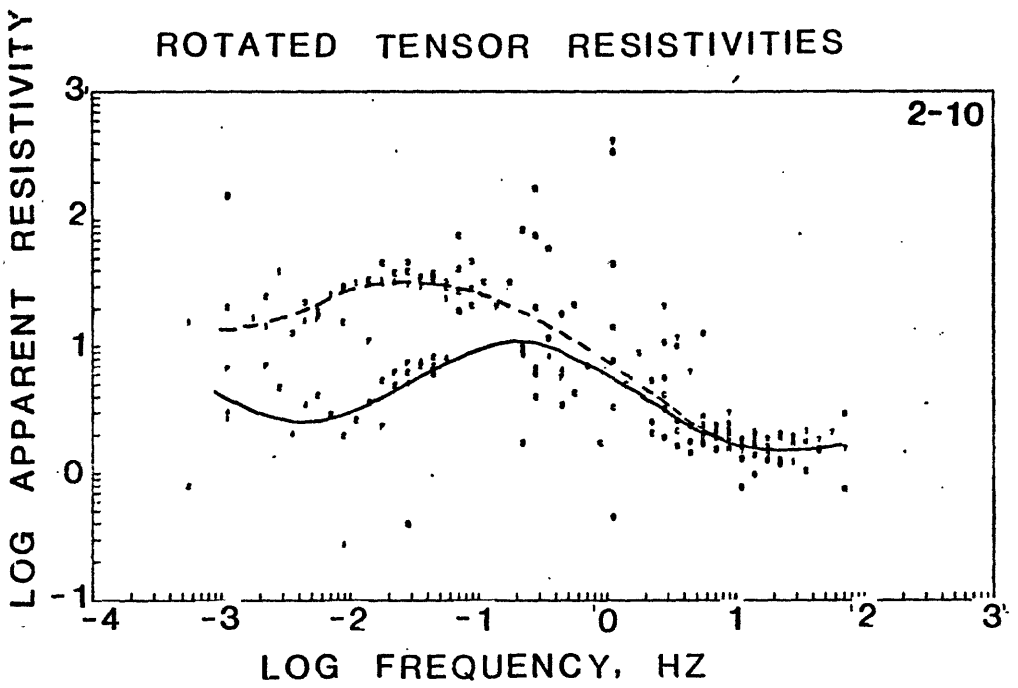
ROTATED TENSOR RESISTIVITIES
2-10
LOG APPARENT RESISTIVITY
3
2
1
0
-1
-4
-3
-2
-1
0
1
2
3
LOG FREQUENCY, HZ

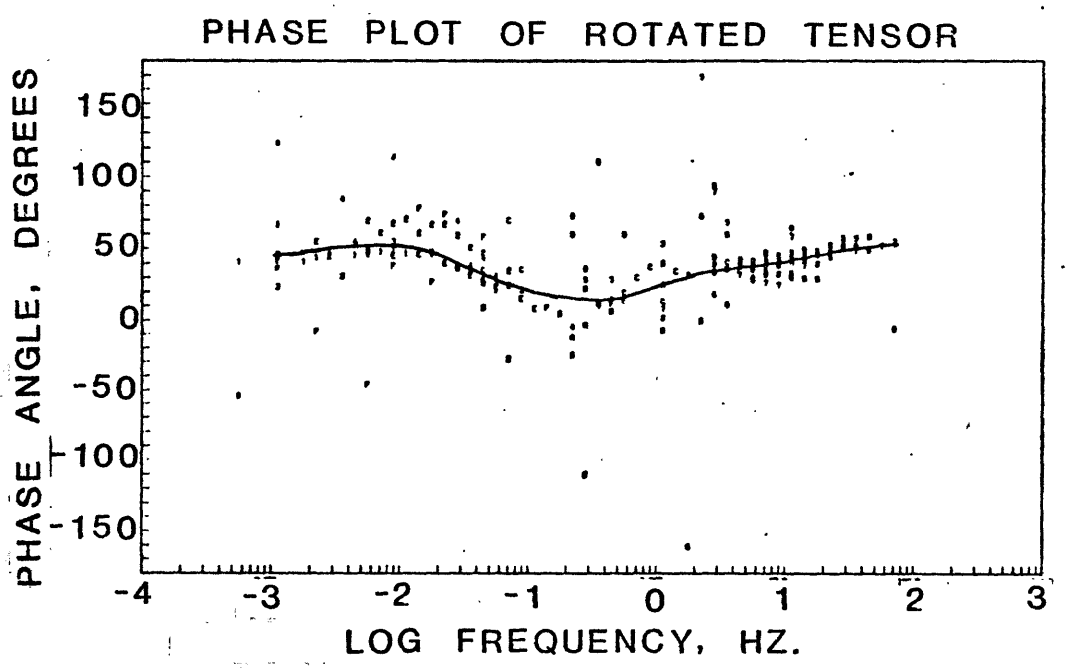
PHASE PLOT OF ROTATED TENSOR
PHASE ANGLE, DEGREES
150
100
50
0
-50
-100
-150
-4
-3
-2
-1
0
1
2
3
LOG FREQUENCY, HZ.

Scatter in the data is evident, being at the extreme at the lowest frequencies where the degrees of freedom necessary for resolution of frequencies lower than about 0.004 Hz was insufficient for good spectral estimates. Also, scatter is quite bad in the region from .2 Hz to 8 Hz, a known null in natural electromagnetic activity. However, even though there are many "flyers" in the data, the resistivity curves are adequately defined except possibly at site 2-10.

The fifteen sets of data from sites 1-1 through 1-15 which did not include a run of band 2 (Table 1) were poorer in quality than that from sites 2-1 through 2-10. There are several reasons for this:

(1) Eight sites were in an irrigation area near Stillwater and significant power-line and other electrical noise existed.

(2) The inductions coils, which should be buried for thermal and vibrational stability, were not given nearly as long to stabilize.

(3) The 1-n sites were done before the 2-n sites during a period of somewhat low natural activity. Also some electronic problems in the MT system were not located until near the completion of the 1-n sites.

We show four typical amplitude curves in figure 4 for the "high frequency" (1-n) sites. The design of these soundings was to obtain as many sites as possible in the short period of time allotted for the survey in order to look at details near the known thermal anomalies. Even though the data were scattered, useful information was obtained and cross-sections compiled from one-dimensional inversion of the amplitude curves appear to be valuable.

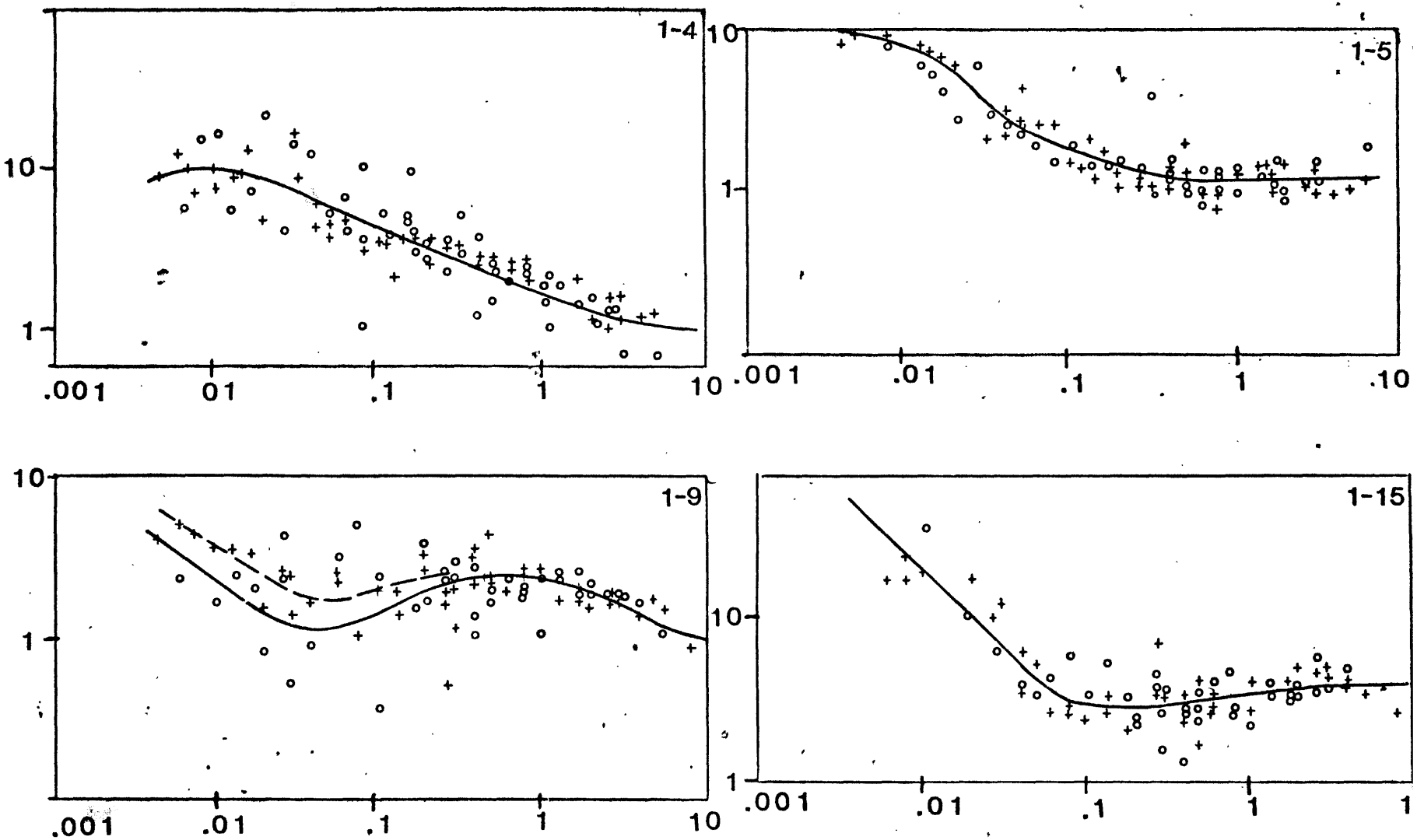

Figure 4.--Tensor resistivity amplitude curves for MT sites 1-4, 1-5, 1-9 and 1-15. Crosses are TE data, circles TM. Horizontal axes are log frequency, vertical axes are apparent resistivity in ohm-metres.

Geology and Thermal Regime: The general geology of the Carson Basin region is shown in plate 1 with 5 mgal Bouguer gravity contours from data

Plate 1 in map pocket

obtained by Wahl (1965) and additional data obtained for this study. The Stillwater-Soda Lake K.G.R.A. is located in the south-central part of the basin (fig. 1). Basaltic rocks of Quaternary age are exposed at several places within the basin. Rattlesnake Hill, just NE of Fallon is probably a basaltic neck or plug. Upsal Hogback is a cluster of several cones of basaltic tuff 16 km north of Fallon. The eruptions that formed these cones occurred chiefly during Late Pleistocene (Morrison, 1964, p. 100). Soda and Little Soda Lakes, 10 km NW of Fallon are small lakes located in basaltic craters. Morrison (1964, p. 72) believes these latter craters overlap the Upsal Hogback features in age.

Extensive shallow drilling (to about 40 m) done by the U.S.G.S., U.S. Bureau of Reclamation, and Standard Oil Co. of California have provided holes for temperature, thermal gradients, and water quality measurements. (Olmstead, et. al., 1975). Considerable information had been available prior to this in the Stillwater area from water wells, but little was known about the Soda Lake thermal anomaly except that steam had been found at 60 m in a well. The steam had been used in the past at a bath house near the well site.

DEPARTMENT OF THE INTERIOR
UNITED STATES GEOLOGICAL SURVEY

OPEN-FILE REPORT
No. 76-80

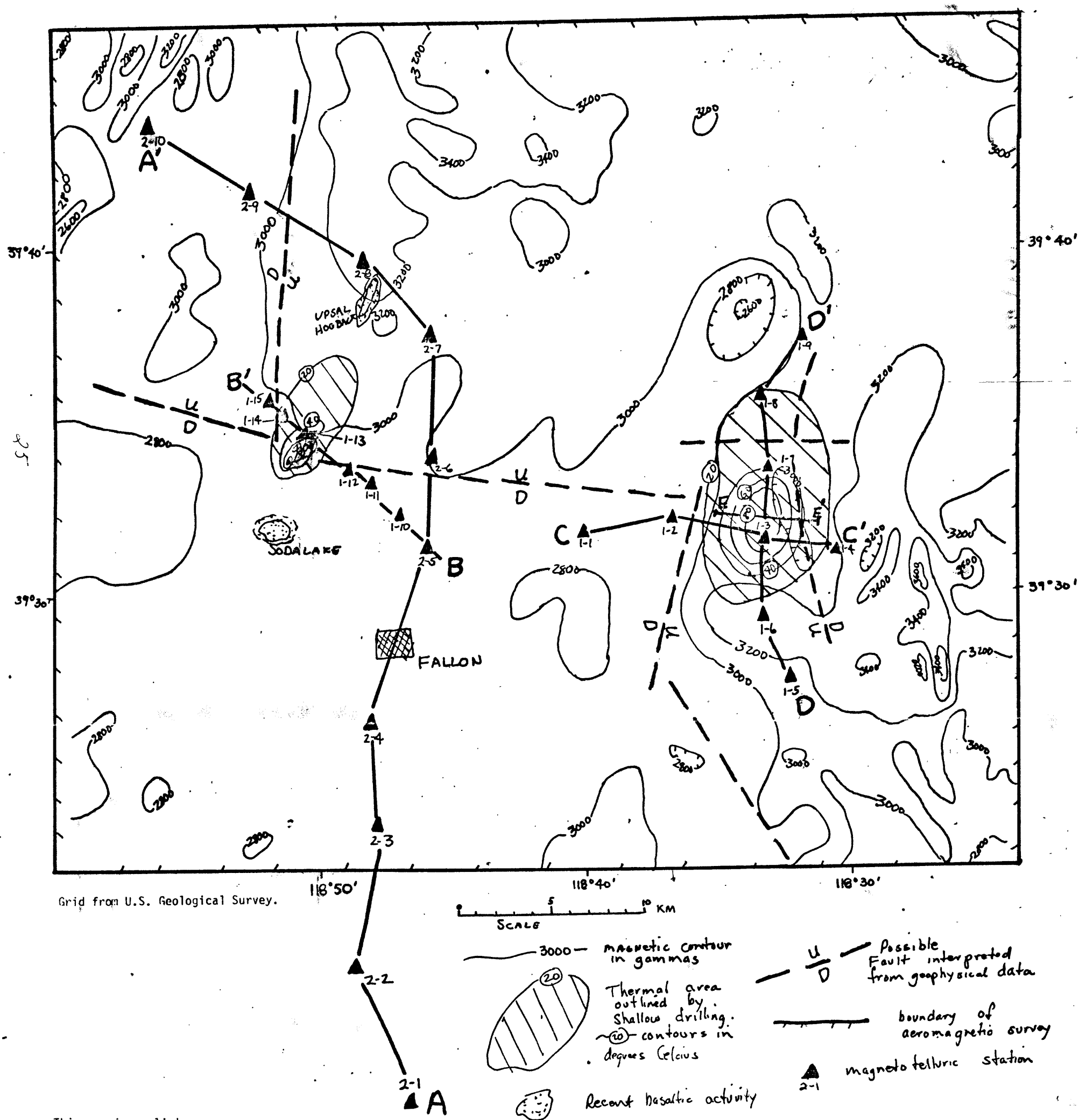

Grid from U.S. Geological Survey.

This map is preliminary and has not been edited or reviewed for conformity to Geological Survey standards.

Figure 5.--Magnetic map, thermal features, and location of MT sites for the Snillwater-Soda Lakes K.G.R.A.

The temperature distribution in the upper 30 metres as determined by drilling in the Stillwater and Soda Lake thermal anomalies is shown in figure 5. Drill holes located between the two thermal areas rule out interconnection at shallow depths.

Both of the thermal anomalies are elongated to the north and this stretching of the isotherms follows the general direction of ground water flow in the area, which is NE along the axis of the basin to a drainage low. An additional factor is that water is probably coming up from depth along north and NE trending faults. This is particularly evident in the thermal area north of Soda Lake, where the innermost isotherms are aligned with the trend between the basaltic centers at Soda Lakes and those at Upsal Hogback. A linear snow melt pattern has also been observed by Olmstead, et. al.(1975) in the same direction.

Water samples typically show dissolved solids of 4000-6000 ppm in both the thermal and non-thermal waters from the area with the thermal water being higher in silica, calcium, and flouride, whereas the non-thermal water is higher in bicarbonate. Reservoir temperatures estimated by silica-quartz and NaKCa geothermometers are 140-160^{o} C (Mariner et. al., 1974).

Gravity and Magnetic Data

The gravity data shown in plate 1 are complete Bouguer gravity values computed with an assumed density of 2.67 gm/cc^3. Contours were generated on the computer using an automatic contouring routine.

A large low with a closure of about 25 mgals just north of the Desert Range is caused by thick unconsolidated alluvium and lacustrine sediments. Previous modeling by Wahl (1965) indicates a maximum thickness of 2 km for the fill, but the magnetotelluric interpretations suggest that the sediments are closer to 3 km thick. The volcanic ranges do not appear to give rise to significant anomalies due to their intermediate density values. In general, large gradients are due to density contrasts between gabbroic rocks (pre-Tertiary section), Tertiary and pre-Tertiary sedimentary sequences, Tertiary and Quaternary volcanics, and unconsolidated sediments, which form a descending sequence of densities. There appear to be no gravity anomalies related to either of the thermal areas.

Aeromagnetic data were obtained with U.S.G.S. aircraft at an elevation of 1.8 km and flight line spacing of 1.6 km. The data were not corrected for the IGRF field and no processing was done except for adjustments to baseline. The hand-contoured data are presented in plate 2. Depth calculations from the magnetic anomalies using half-width formulas provide an estimate of 2-4 km to the source of the anomalies. The sources are within the Tertiary and Quaternary volcanic sections and possibly in buried intrusives. A simplified version of the magnetic map is shown in figure 5.

MT Cross-Sections

The four geoelectrical cross-sections constructed from the MT one-dimensional inversions are shown in figure 6 and 7. We have made some generalizations about what we think the electrical layers represent in terms of geologic units:

The unconsolidated basin sediments of Tertiary and younger age are represented by the 1-5 and 5-20 ohm-m (sand pattern) layers. Along section A-A' (location on fig. 5), there is a maximum of about 2.5 km of 1-5 ohm-m unconsolidated sediments at site 2-3. The 5-20 ohm-metre material at the surface from about site 2-7 to 2-10 (but below surface at 2-9) on section AA' probably consists mostly of basaltic ashes and tuffs from vents at Upsal Hogback. The 1-5 ohm-m sediments are probably mostly playa type deposits of Quaternary age with high percentages of clay. On section CC' (location on fig. 5) the 5-20 ohm-m material is beneath the 1-5 ohm-m material and probably represents Tertiary age unconsolidated sediments. Although the data for the C-C' sites were of poor quality, our cross-section agrees quite well with a geologic section from Olmstead et. al. (1975) shown in figure 8. Olmstead interprets a section of Tertiary alluvium of about 1 km thickness. His section used stratigraphic and temperature information from a private geothermal test (to 1292 m) near the center of the area. Unfortunately no electrical logs are available for this well. The thickness of unconsolidated materials on the upthrown

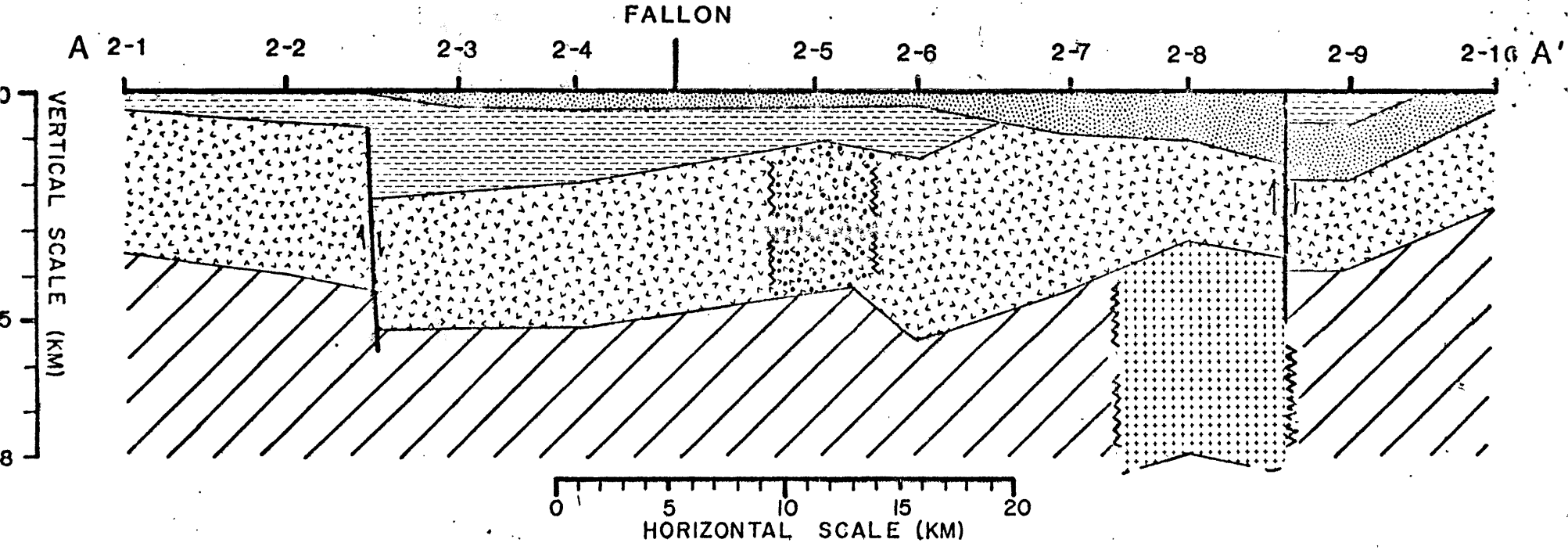

OHM-M	PROBABLE GEOLOGY
<1	Tertiary and pre-Tertiary sediments
1-5	Playa sediments, Quaternary
5-20	Aeolian sediments and ashes
5-20	altered volcanic rocks, Tertiary
20-50	Tertiary volcanics rocks
>50	Quaternary volcanic rocks and intrusives

Figure 6.--MT cross-section AA'

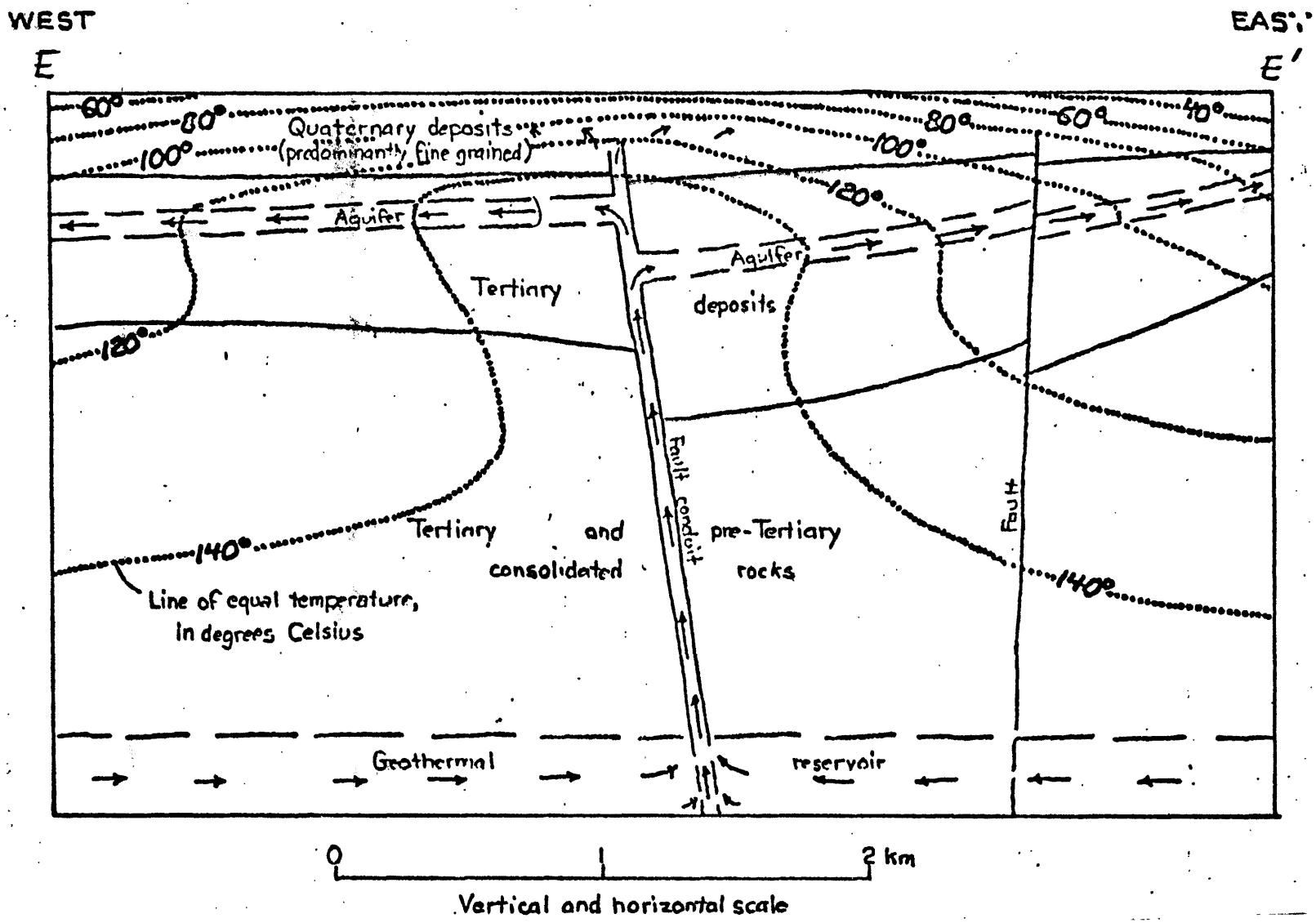

Figure 8.--Geologic cross-section through Stillwater thermal area; from Olmstead, et. al. (1975). Location of cross-section is shown on fig. 5.

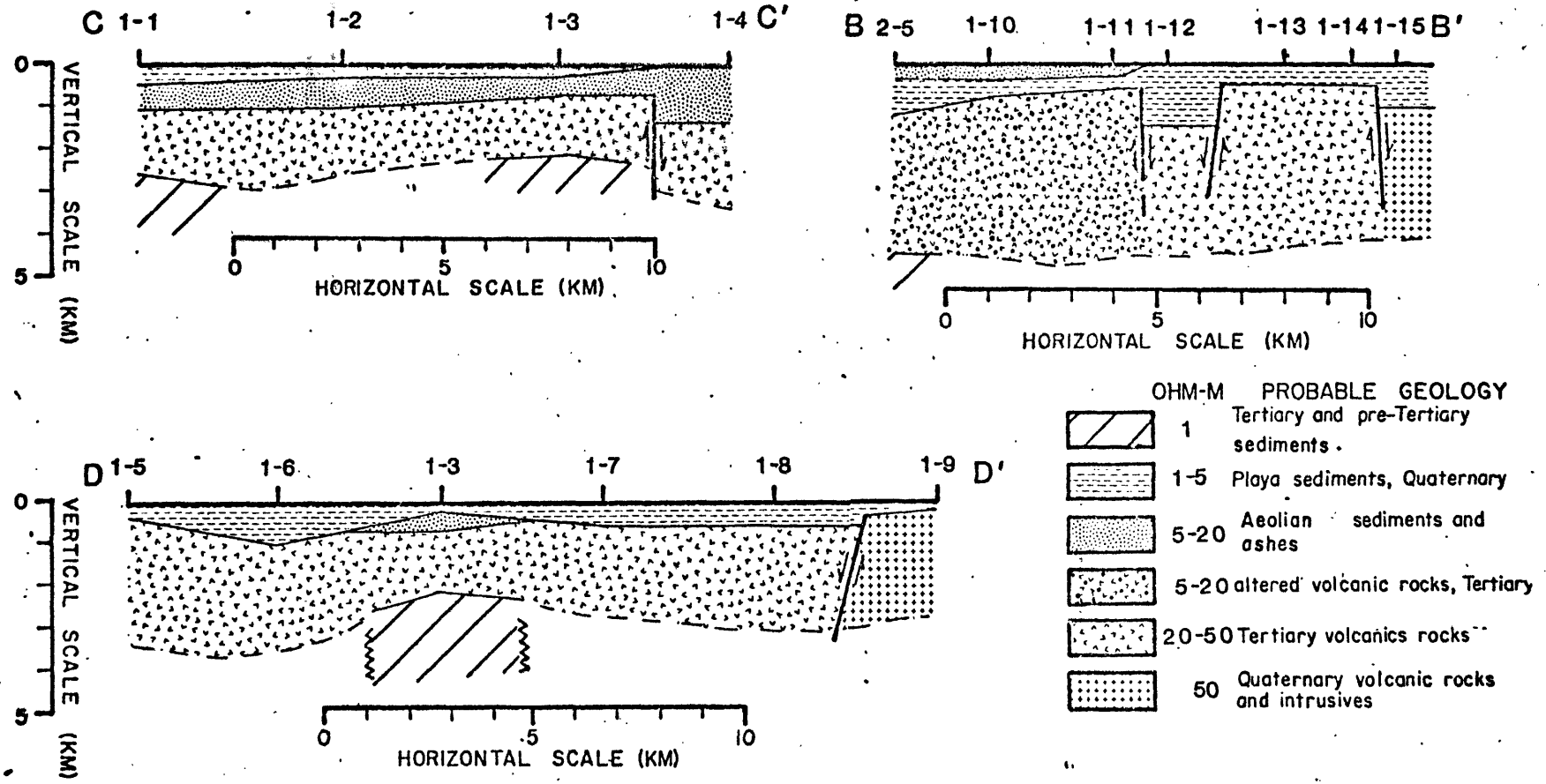

Figure 7.--MT cross-sections BB', CC', and DD'

and downthrown sides of the fault between 1-3 and 1-4 agree well with Olmstead's section. Note that on figure 5 there is an aeromagnetic low in the central part of Stillwater thermal anomaly that coincides with the faults shown on MT section CC' and Olmstead's geologic section (fig. 8). This implies that hot water rising along the fault has converted magnetic minerals to non-magnetic ones by hydrothermal alteration. This has probably taken place in the Tertiary volcanic rocks in the vicinity of the fault.

The 20-50 ohm-metre layer is generally thought to represent Tertiary volcanic rocks which probably flooded the developing Carson basin to large thicknesses. The sounding curves along section A-A' could be approximated quite easily with resistivities of about 30 ohm-m for this layer, except at site 2-5, where we were forced to use a resistivity of less than 10 ohm-m. In addition, at sites 1-10 and 1-11 resistivities of about 10 ohm-m seemed to be called for. These lower resistivities may be caused by an area of extensive alteration in the volcanic rocks. We have suggested this possibility on the cross-section by using an alteration pattern superimposed on the layer at these sites. The interpretation of data from site 2-8 suggest a resistive zone at depth that does not show up on any of the other curves. The volcanic activity at Upsal Hogback, near site 2-8, and the occurence of an aeromagnetic high (figure 5) and the high resistivity unit at depth suggest that an intrusive may exist at about 4 km beneath site 2-8. The linear truncation of the aeromagnetic high and the change in upper unit depth (the extension of the 5-20 ohm-m layer to a depth of 2.5 km at site 2-9) suggest to us that normal faulting has occurred on the west side of the intrusive as shown on Section A-A'.

The most significant part of the geoelectrical section is the layer of less than 1 ohm-m interpreted to occur at depths of 4 to 7 km along most of section A-A' and possibly at depths of about 2.5 km along section C-C'. This layer probably consists of Tertiary and pre-Tertiary marine sediments saturated with water of 150° C or greater and salinities of about 20,000 ppm. Using a temperature of 150° C, salinity of 20,000 ppm, and formation factor of 10 as reasonable estimates of formation properties, we calculate a formation resistivity of 0.8 ohm-m, which seems compatible with most of the MT section along section A-A'. The figure of 150° C is taken from estimates of reservoir temperatures using geothermometric data and probably represents a minimum temperature for the anomalous zone. The salinity of 20,000 ppm is an estimate of what might be expected in pre-Tertiary marine sediments which haven't been flushed. In addition, the high temperatures may mean that formation salinities are even higher due to increased solubility. Higher salinities and higher temperatures, would of course mean lower formation resistivities. From the MT data we can only state that formation resistivities must be less than 1 ohm-m, but 0.3 to 0.8 ohm-m seems the be the most reasonable range. The figure of 0.3 ohm-m corresponds to a salinity of 60,000 ppm using the estimated minimum temperature of 150° C and formation factor of 10. Actual temperatures in the conductive zone are probably in the range of 150-350° C.

The only heat-flow data available are from an experimental heat-flow test hole near the middle of the Carson Sink, 43 km northeast of Fallon. The test hole was drilled to a depth of 153.9 m and had a heat flow of 1.57 HFU (heat flow unit:cal $cm^{-2}s^{-1}x10^{-6}$) calculated from the measured thermal gradient. The corrected heat flow using an estimated rate of deposition of playa sediments of 1 mm/year, was determined to be 1.9 HFU (Olmstead, et. al., 1975). This value is only slightly anomalous, being about a mean for the northern Basin and Range. It is not as high as for instance, values obtained over a large area around Battle Mountain, Nevada (Sass, et. al., 1971), which range from 2.5 to 3.8 HFU. Upward convection will bias heat-flow values to the high side, and since there appears to be no evidence for convection in the nature of hot springs in the test hole area, we suspect that the heat flow measurement is not biased excessively upward. However, the measurement may be biased downward by lateral flow of ground water in the area. The test hole was in the Carson Sink, the center of drainage for the closed Carson Desert basin. Water table surface measurements by Olmstead et. al., (1975) show that groundwater flow is toward the Carson Sink. This influx of cold water probably biased the heat-flow measurement down, if the measurement is biased at all.

Olmstead has calculated an estimated depth of circulation for recharge water in a hypothetical area of 2 HFU and with no shallow crustal heat source. Recharge water must circulate to depths of 2-6 km in such a system to be heated to 160-200^{o} C, depending on the thermal conductivity of the rocks. This range overlaps the depth to the conductive layer from the MT cross-sections of 2.5-7 km. The heat flow data, geothermometric data, and magnetotelluric data suggest temperatures in excess of 150^{o} C at depths of 2-7 km. Rocks at these depths are probably predominately sedimentary rocks with highly saline pore waters which are capped by more impermeable Tertiary volcanic flows. The only access to the hot water bearing rocks is along Basin and Range faults, which provide both recharge and discharge paths. Modeling of the data at MT sites 2-1 to 2-3 indicates the low resitivity rocks are at least 2.5 km thick in this area, assuming a resistivity of 0.5 ohm-m.

SUMMARY AND CONCLUSIONS

The occurence of low resistivity rocks at depths of 2.5-7 km over much of the survey area suggests a major thermal anomaly exists in the Carson Desert region. There is no problem justifying the low resistivities observed if we assume a rock temperature in excess of 150^{0} C and salinities in excess of 20,000 ppm. Figure 5 shows the position of major faults which we interpret as possiblities from the aeromagnetic and MT data. We have not shown a fault running between Upsal Hogback and Soda Lake, although all evidence other than the geophysics points to its existence. Olmstead points out that over parts of the area, a shallow sand aquifer (see figure 8) distributes the thermal waters rising from the deep reservoir. The self sealing and/or fracturing of this aquifer probably plays the major role in determining where the hot water reaches the near surface. Thus the hydraulic connection between major normal faults and near surface fractures may not be a simple one.

The MT data do not seem to indicate any major resistivity anomalies in the upper 1 km of unconsolidated sediments that may be associated with the mapped thermal anomalies. This is probably because resistivities are normally very low in the clay sediments and the variation in clay content and salinity is more important in determining resistivities than water temperature. Also, the salinity of the thermal water appears to be about the same as that of the non-thermal water.

The widespread occurence of the low resistivity rocks suggests to us that the anomalous heat comes from a deep, broad area of hot crust, rather than from localized intrusive heat sources. This thermal anomaly is probably related to anomalously thin crust (24 km) found in seismic refraction studies (Pakiser and Hill, 1963).

References

Mariner, R. H., Rapp, J. B., Willey, L. M., and Presser, T. S., 1974, The chemical composition and estimated minimum thermal reservoir temperatures of the principal hot springs of nothern and central Nevada: U.S. Geol. Survey Open File Report.

Morrison, R. B., 1964, Lake Lahontan: Geology of the southern Carson Desert, Nevada: U.S. Geol. Survey Prof. Paper 401.

Olmstead, F. H., Glancy, P. A., Harrill, J. R., Rush, F. E., and VanDenburgh, A. S., 1975, Preliminary hydrogeologic appraisal of selected hydrothermal systems in northern and central Nevada: U.S. Geol. Survey, Open File Report 75-76.

Pakiser, L. C. and Hill, D. P, 1963, Crustal structure in Nevada and Southern Idaho from Nuclear Explosions: Jour. Geoph. Res., Vol. 68, No. 20 p. 5757-5766.

Sass, J. H., Lachenbruch, A. H., Munroe, R. J., Greene, G. W., and Moses, T. H., Jr., 1971, Heat flow in the Western United States: Jour. Geophys. Research, v. 76, no. 26, p. 6376-6413.

Schrader, F. C., 1947, Carson Sink area, Nevada: U.S. Geol. Survey Open File Report, Mackay School of Mines, U. of Nevada, Reno.

Sims, W. E., Bostick, F. X., Jr., and Smith, H. W., 1971, The estimation of magnetotelluric impedance tensor elements from measured data: Geophysics, vol. 36, no. 5, p. 938-942.

Wahl, R. R., 1965, An interpretation of gravity data from the Carson area, Nevada: Student report, Dept. of Geophysics, Stanford University.

Webb, Barbara, and Wilson, R. V., 1962, Progress geologic map of Nevada: Nevada University, Nevada Bur. Mines Map 16.

Word, D. R., SMith, H. W., and Bostick, F. X., Jr., 1969, An investigation of the magnetotelluric tensor impedance method: EERL Tech. Rep. No. 82, U. of Texas at Austin.